Élise DELHEZ

Experimental and numerical modal analyses of a pre-stressed steel strip

December 2017

Contents

List of Figures

List of Tables

Introduction

This work is devoted to the modal analysis of a pre-stressed steel strip. Two different complementary approaches exist in modal analysis, respectively the theoretical and experimental modal analyses. On the one hand, the theoretical modal analysis is related to a direct problem. It requires a model of the structure. Model uncertainties are inherent to this kind of analysis. On the other hand, the experimental analysis is an inverse problem and requires a prototype. It allows to check if the finite element model represents reality in an accurate way and to assess the impact of model uncertainties. It is important to highlight that modal analysis relies on two important assumptions: linearity and time invariance of the structure. Even if these assumptions are never perfectly met in practice, they are not far from reality.

The flowchart represented in Fig. 1 summarizes the basics of the "model updating scheme" followed in this report. The methodology is inspired from those described in [5] and [6]. Starting from a real structure, the two complementary modal analysis approaches are followed. The first section is devoted to the theoretical modal analysis of the structure. A finite element model of the structure is built and allows to evaluate the modal properties of the strip. The results of this first section are then used to prepare the experimental measurements. The experimental modal analysis, described in section 2, allows to get a second evaluation of the modal characteristics of the structure. In the third section, the results from both the theoretical and experimental modal analyses are compared with each other and the finite element model is eventually updated in order to get a reliable model that reproduces the experimental results in an accurate way.

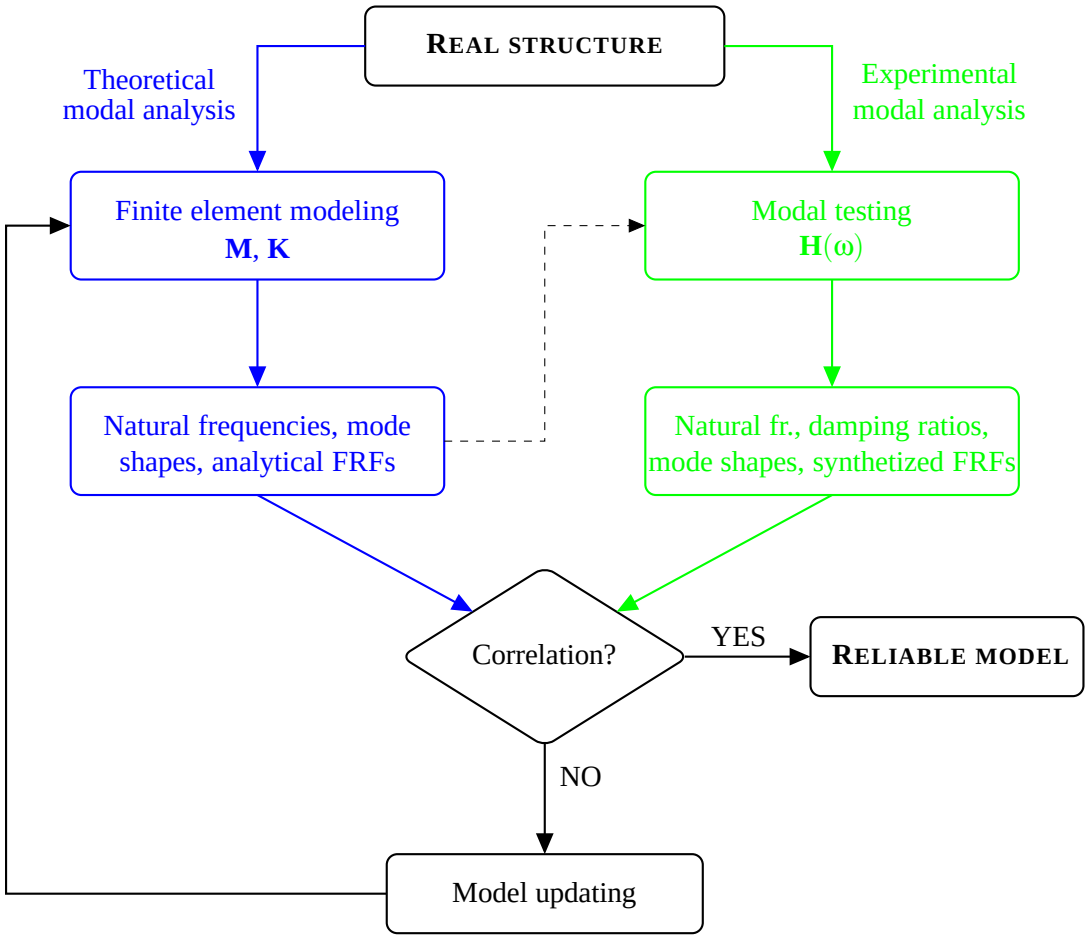

FIGURE 1 - Model updating scheme.

1 Finite element analysis

In this first section, finite element models of the structure are built in MATLAB and SAMCEF Field. These models are used to get a first evaluation of the natural frequencies and mode shapes of the structure.

The studied structure consists in a vertical strip fixed at its extremities, as represented in Fig. 2. The geometrical dimensions of the strip used in this first finite element model are listed in Table 1. The strip is pre-stressed by a mass of 1.8 kg.

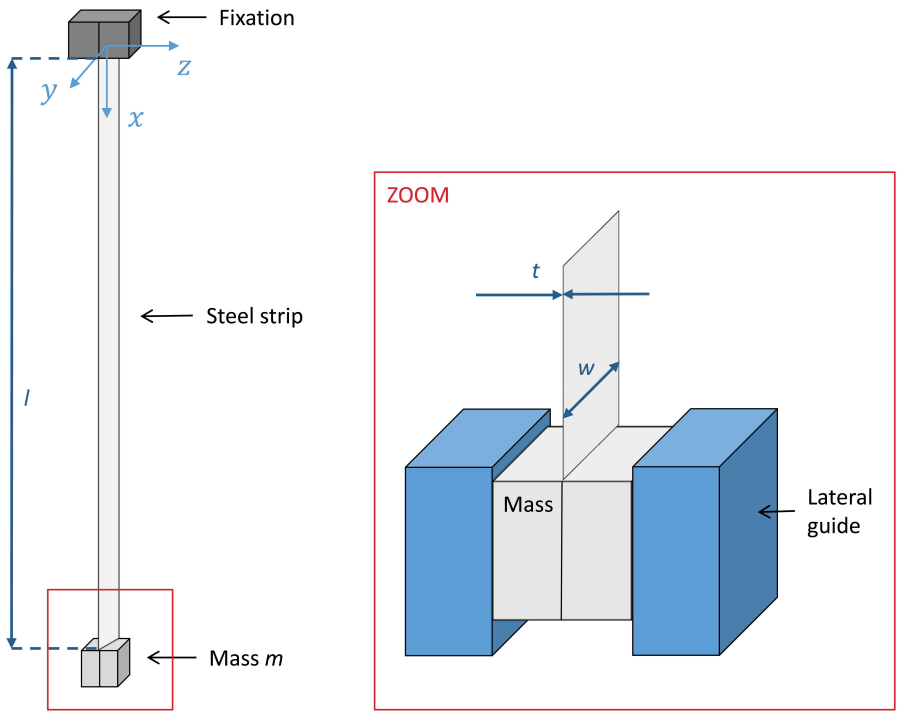

FIGURE 2 - Schematic view of the structure.

Parameter	*Symbol*	*Value*	*Units*
Length	l	50	cm
Width	w	25	mm
Thickness	t	0.4	mm
Pre-stress mass	m	1.8	kg

TABLE 1 - Main properties of the steel structure.

The material properties of the steel used in the model correspond initially to a standard steel [1] (see Table 2).

The structure is modeled in MATLAB using Bernoulli beam elements. The strip is divided into constant size elements. The mass and stiffness matrices **M** and **K** are obtained by assembling the corresponding element matrices. It should be noted that the stiffness matrix is composed of two parts: a geometrical stiffness

Parameter	*Symbol*	*Value*	*Units*
Density	ρ	7,800	kg/m^3
Young's modulus	E	210	GPa
Poisson's ratio	ν	0.3	[-]

TABLE 2 - Material properties of the steel structure.

matrix is added to the usual linear stiffness matrix to take into account the increased stiffness induced by the pre-stress mass. The element matrices used in the implementation of the finite element model can be found in [4]. Regarding the boundary conditions, the strip is assumed to be perfectly clamped at its top extremity. At its bottom, a lateral guide allows the strip to move only in the vertical x direction (see Fig. 2).

A similar model is built in SAMCEF Field.

These two finite element models are used to compute the seven first natural frequencies of the strip. These frequencies are listed in Table 3. Both models use 50 elements of 1 cm length. It is checked at the end of the section that this discretization is sufficient to capture the dynamics of the problem. The results obtained with the two models are in good agreement, which gives confidence in the MATLAB model and in the way in which pre-stress is taken into account. The results also confirm that Bernoulli elements are appropriate for representing the dynamics of the strip. The relative errors between these frequencies computed with the two models can be partially ascribed to the different treatments of shear deflection in the two approaches. The maximal relative error is indeed obtained with the fifth mode which is, as shown below, the first torsion mode of the structure.

	Frequency [Hz] MATLAB	*Frequency [Hz]* SAMCEF Field	*Relative error [%]*
Mode 1	18.35	18.37	0.10
Mode 2	39.76	39.79	0.07
Mode 3	66.14	66.16	0.03
Mode 4	98.65	98.66	0.01
Mode 5	102.96	103.55	0.57
Mode 6	137.88	137.89	0.01
Mode 7	184.16	184.18	0.01

TABLE 3 - Eigenfrequencies obtained with elements of 1 cm in length.

The corresponding mode shapes (obtained with the MATLAB model) are represented in Fig. 3. The modes obtained with the SAMCEF Field model (not shown) are similar. The higher the natural frequency, the more complex the form of the mode shape. The fifth mode is a torsion mode around the x-axis while the six other modes are the successive bending modes around the y-axis. Those are the usual low-frequency modes for a beam.

In the absence of accurate information about damping, the damping ratios corresponding to the identified modes are not estimated with the finite element model. Only the experimental measurements described in the next section can provide reliable estimates.

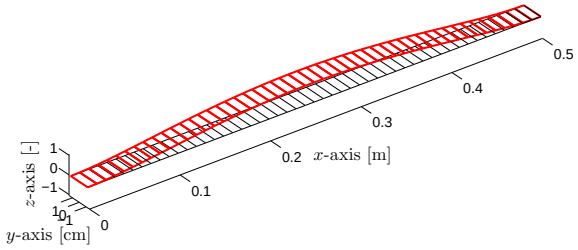

(a) Mode 1.

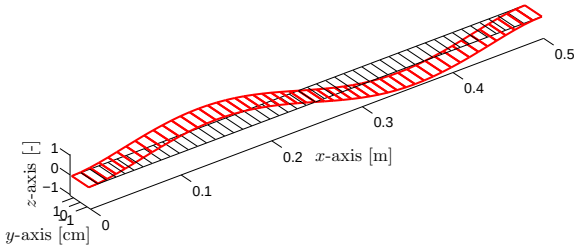

(b) Mode 2.

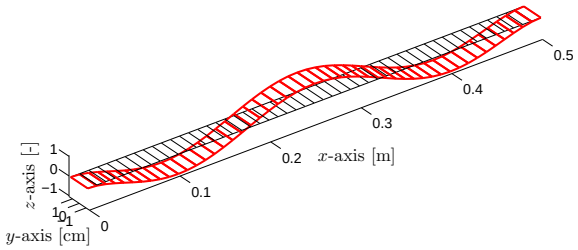

(c) Mode 3.

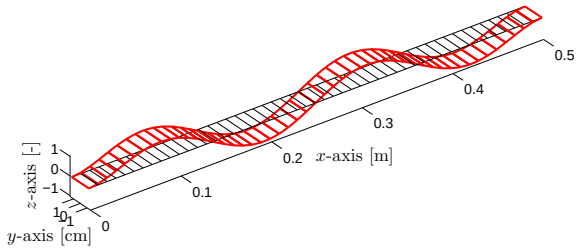

(d) Mode 4.

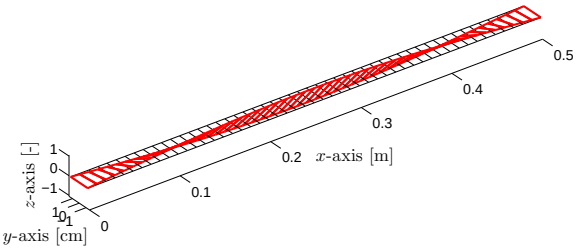

(e) Mode 5.

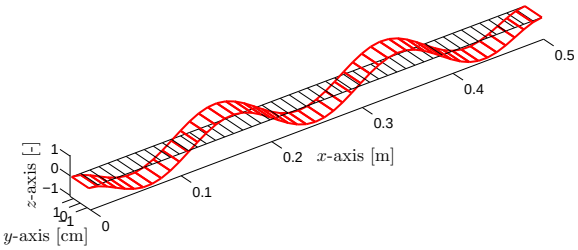

(f) Mode 6.

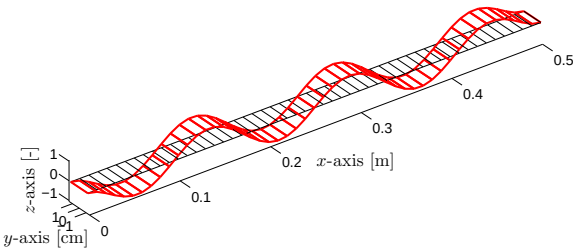

(g) Mode 7.

FIGURE 3 - The seven first modes of vibration obtained in MATLAB.

Before further analyzing the structure, it is checked that the finite element discretization is sufficient to capture the dynamics of the strip up to its seventh mode. Fig. 4 shows the eigenfrequencies computed with the MATLAB model using different numbers of elements. The different results are normalized by the eigenfrequencies computed with 50 elements, as listed in Table 3. Although the torsion frequency (mode 5) converges slightly more slowly, it can be checked that the different eigenfrequencies do not significantly change when the number of elements is increased beyond 50, *i.e.* for elements of length smaller than 1 cm. This finite element resolution is therefore considered as appropriate.

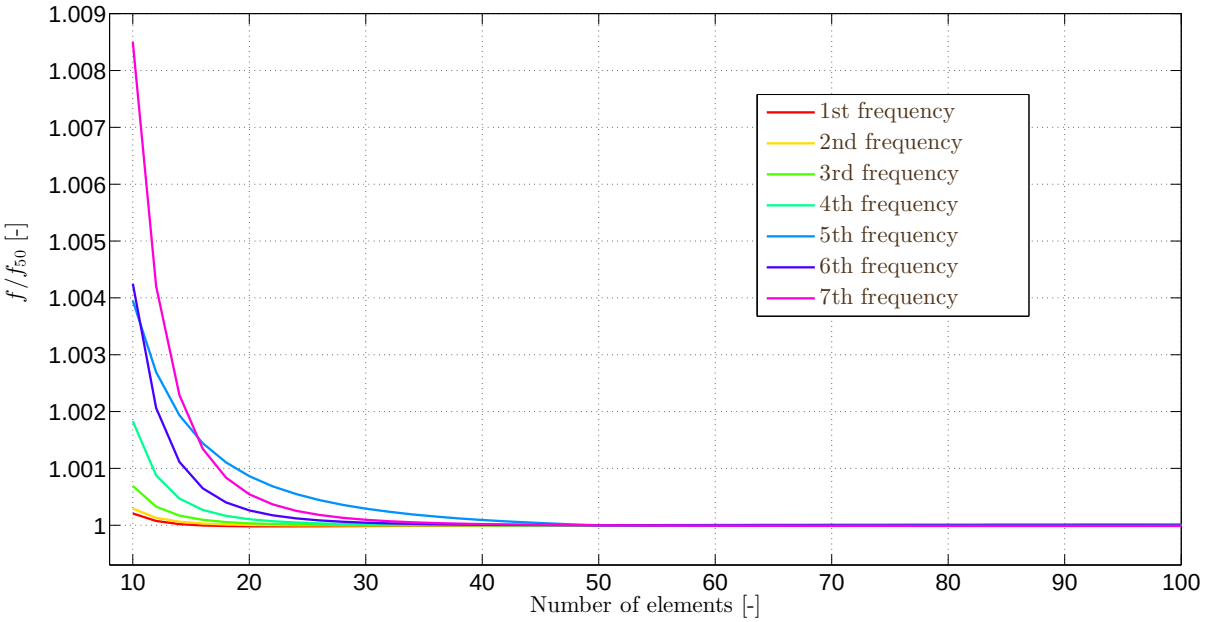

FIGURE 4 - Natural frequencies normalized by the natural frequencies computed with 50 elements as a function of the number of elements.

2 Experimental modal analysis

This section presents the methodology and the main results of the experimental modal analysis of a physical prototype of the structure. First, the main components of the measurement chain are described together with the signal processing parameters. Then, a preliminary data acquisition is performed in order to get a first idea of the modal parameters of the strip. Eventually, a more detailed data acquisition is carried out and the modal parameters of the structure are identified.

2.1 Measurement process

Before going further in the analysis, the main components of the measurement chain are described. The different signal processing parameters are also described and justified.

The first element of the measurement chain is the tested structure described in section 1. The experimental set-up is pictured in Fig. 5. The finite element analysis performed in the previous section can help to prepare the measurement process. In the following, the focus is put on the bending modes of the structure. There is therefore no need to consider measurement or excitation points that are not located on the central fibre of the strip. In order to correctly represent the dynamics of the six first bending modes identified in Fig. 3, 9 equally spaced points on the strip are considered (see Fig. 6). These points are denoted by P1 to P9 in this report.

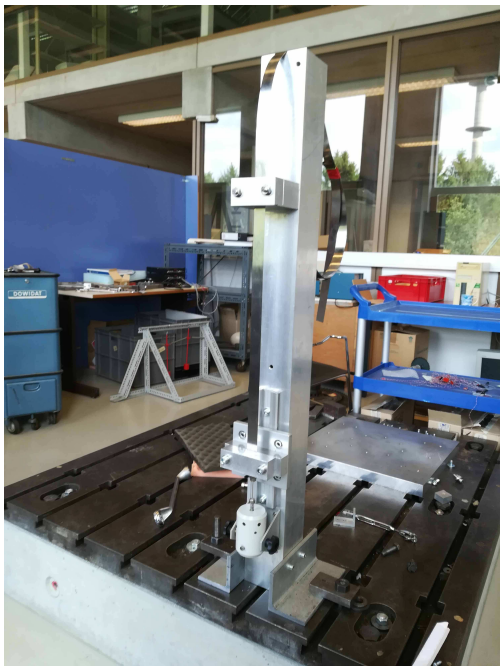

FIGURE 5 - Experimental set-up.

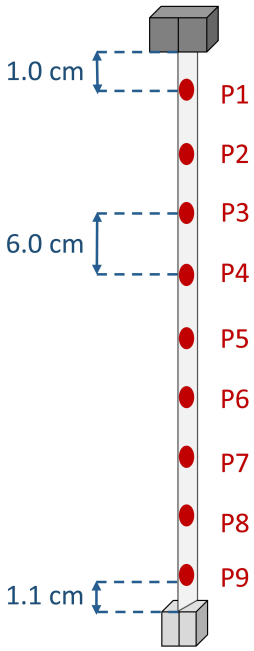

FIGURE 6 - Excitation and measurement points.

The data acquisition and signal processing are carried out using the LMS SCADAS Mobile acquisition system and the LMS Test.Lab software [6]. All the modes of interest have frequencies less than 200 Hz. In order to avoid aliasing error, a bandwidth of 400 Hz is chosen. This is justified further. In order to reach an accuracy close to 0.1 Hz on the frequencies, 4096 spectral lines are considered. This gives an acquisition time of 10.24 s.

An impact hammer is used to excite the structure. This is indeed the simplest way of obtaining the impulse response functions (or equivalently the frequency response functions) required to identify the modal properties of the structure because it does not require to attach anything to the structure, which would not be appropriate considering the small weight of the steel strip. The hammer includes a force transducer. Its main characteristics are given in Table 4.

Sensitivity	2.23 mV/N
Transducer type	086B03
Transducer manufacturer	PCB
Serial number	5856

TABLE 4 - Characteristics of the impact hammer.

The studied structure is very light. In order to avoid any overloading of the channels, the amplitude of the force applied has to remain relatively small. The heavy head of the hammer is therefore removed.

The impact hammer can be used with two tips of different stiffness: a steel tip and a vinyl one. For the current application, there is no need to excite the structure at very high frequencies. The vinyl tip, which is softer, is therefore chosen. The power spectral density of a typical impact is represented in Fig. 7. The figure shows that the energy of the impact is well spread over all the frequencies of interest. The analysis of the bandwidth in the LMS Test.Lab software confirms that impacts with this kind of hammer and tip do not excite in a significant way the frequencies beyond 400 Hz. The choice of the tip is therefore appropriate for the current study.

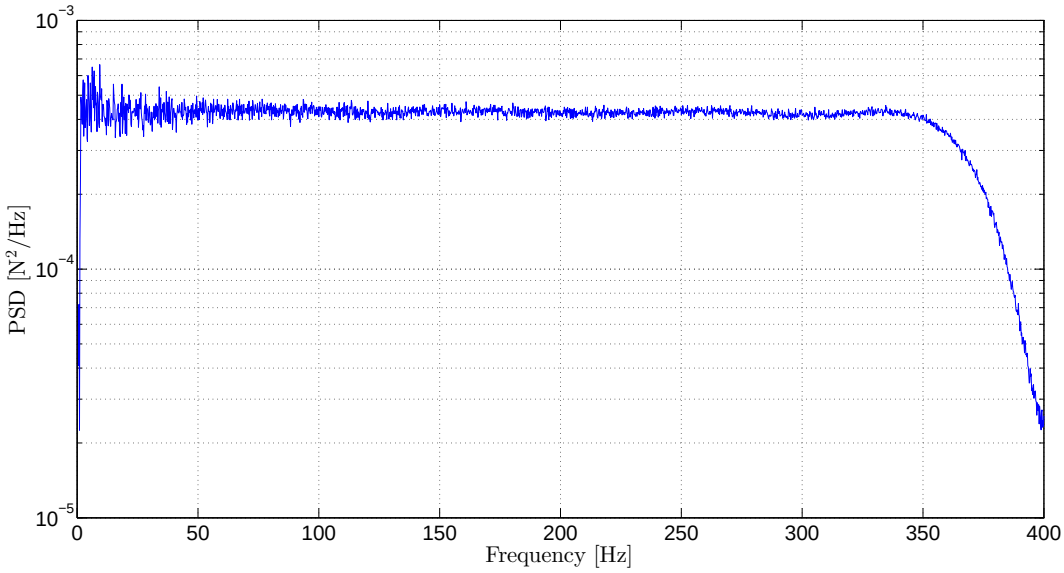

FIGURE 7 - Power spectral density of a typical impact force.

In order to correctly capture the impact, two quantities have to be defined: the trigger level and the pre-trigger. Those are automatically defined by the LMS Test.Lab software by analyzing and averaging several impacts [6]. On the one hand, the acquisition is triggered when the signal on the hammer channel exceeds

the trigger level, which is 0.1 N here. On the other hand, pretrigger determines the time prior to the trigger condition that will be included in the acquisition. It is given by 0.1 s in the considered experimental set-up.

Because the studied structure is very light, it is important to avoid modifying its mass by adding accelerometers on it. The response (in term of velocity) of the structure to the impacts is therefore measured with a laser transducer whose main characteristics are given in Table 5.

Sensitivity	1000 mV/(m/s)
Transducer type	MSA-400 OFV-552
Transducer manufacturer	Polytec
Serial number	0110716

TABLE 5 - Characteristics of the laser transducer.

Also because of its lightness, the structure is very responsive to hammer impacts. In order to avoid any overloading of the channels, the structure is only excited at the point closest to the bottom fixation (point P9 in Fig. 6). The laser transducer is used to measure the response at the different points P1 to P8. A roving accelerometer technique is used to measure a row of the frequency response functions matrix.

When processing the signal, two types of errors may appear: variance and bias errors [3]. Variance errors are due to the discrepancy between the mean of each sample and the mean of the ensemble. Such errors can be reduced by averaging a sufficiently large number of samples. To achieve a good compromise between the acquisition time and the accuracy of the measures, the average between three successive tests is made. Bias errors can be separated into aliasing and leakage errors.

The LMS Test.Lab software set the sampling rate ω_s at a sufficiently high value to avoid aliasing [6]. In order to limit the frequency content beyond $\omega_s/2$, which is folded back in the low frequency range, it is important to avoid triggering modes with frequencies larger than 400 Hz. As stated previously, the chosen hammer/tip combination does not excite in a significant way the frequencies beyond 400 Hz. Since the structure is supposed to be quasi-linear, the frequency content of the response beyond 400 Hz is therefore also small.

In order to reduce leakage errors, windowing techniques are applied to the excitation and the response signals. These windows force the signal to vanish at the end of the observation time and, therefore, filter out otherwise unavoidable noise components at the end of the signal. The forms of the windows are adapted to the forms of the signal: a rectangular window is chosen for the impact and an exponential one for the response. The optimum parameters defining the windows are set by the LMS Test.Lab software by analyzing and averaging several successive impacts [6].

2.2 Preliminary data acquisition

Before embarking upon the complete modal analysis of the strip, the analysis of the response of the structure to a single impact is used to provide a first idea of the natural frequencies and damping ratio's. As explained previously, the structure is triggered at point P9 (see Fig. 6). The measurement point must be carefully chosen in order to detect all the modes identified with the finite element method. It is therefore important that this point does not coincide with a vibration node of any bending mode. The point P2 satisfies this condition and is therefore chosen.

The measured frequency response function and its coherence function are represented in Fig. 8. The coherence function is a good indicator of the accuracy and the repeatability of the performed impacts [5]. The values close to 1 taken by the coherence function in the whole range of interest indicates that the noise in the measured signals is limited and that the three successive impacts are performed accurately at the same location. As expected, the coherence function drops at low frequency and at the anti-resonance frequencies.

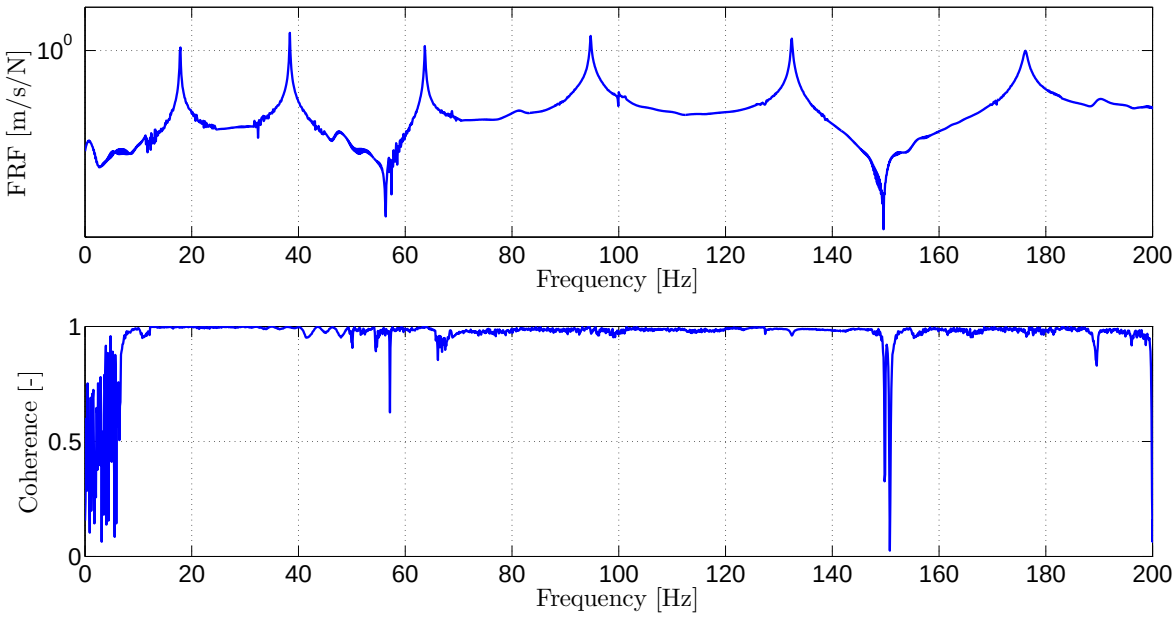

FIGURE 8 - Frequency response function and coherence function corresponding to an excitation at point P9 and the measure of the response at point P2.

The measured frequency response function plotted in Fig. 8 provides a quick way of determining the number of modes in a given bandwidth [3]. It allows to highlight the resonance peaks of the structure and, therefore, to identify the resonance frequencies[1]. Six modes can be clearly seen between 0 and 200 Hz. They correspond to the 6 bending modes identified with the finite element model. The natural frequencies obtained by this analysis of the experimental data are given in Table 6.

	Frequency [Hz]
Bending mode 1	17.9
Bending mode 2	38.3
Bending mode 3	63.7
Bending mode 4	94.7
Bending mode 5	132.4
Bending mode 6	175.5

TABLE 6 - Eigenfrequencies obtained from the frequency response function plotted in Fig. 8.

[1] When a single frequency response function is measured experimentally, the *Complex Mode Indicator Function* provides exactly the same information and is therefore not implemented for the present study.

This preliminary data acquisition can also provide estimates of the damping ratios associated to the different modes. Two single degree of freedom methods are implemented in MATLAB: the peak-picking method and the circle-fitting method. These two methods work in the frequency domain. Single degree of freedom modal analysis methods may be applied when the modes are well separated in frequencies and can therefore be analyzed separately by focusing on a given frequency bandwidth. The accuracy of the peak-picking method and the circle-fitting method depends on the number of points that describe the resonance peak. These methods are used here to estimate the damping ratio of the fifth bending mode, because the related peak is the most accurately described in the measured FRF. Similar results can be obtained for the other modes of the structure.

The peak-picking method is illustrated in Fig. 9 [5]. In this figure, the peak corresponding to the fifth bending mode is isolated. The Bode plot of the FRF amplitude is used to detect the maximum response and the half-power points. The modal damping is evaluated by

$$\zeta \simeq \frac{\Delta f}{2f}, \tag{1}$$

where Δf is the frequency bandwidth between the half-power points and f is the natural frequency of the mode (see Fig. 9). A damping ratio of 0.09% is found.

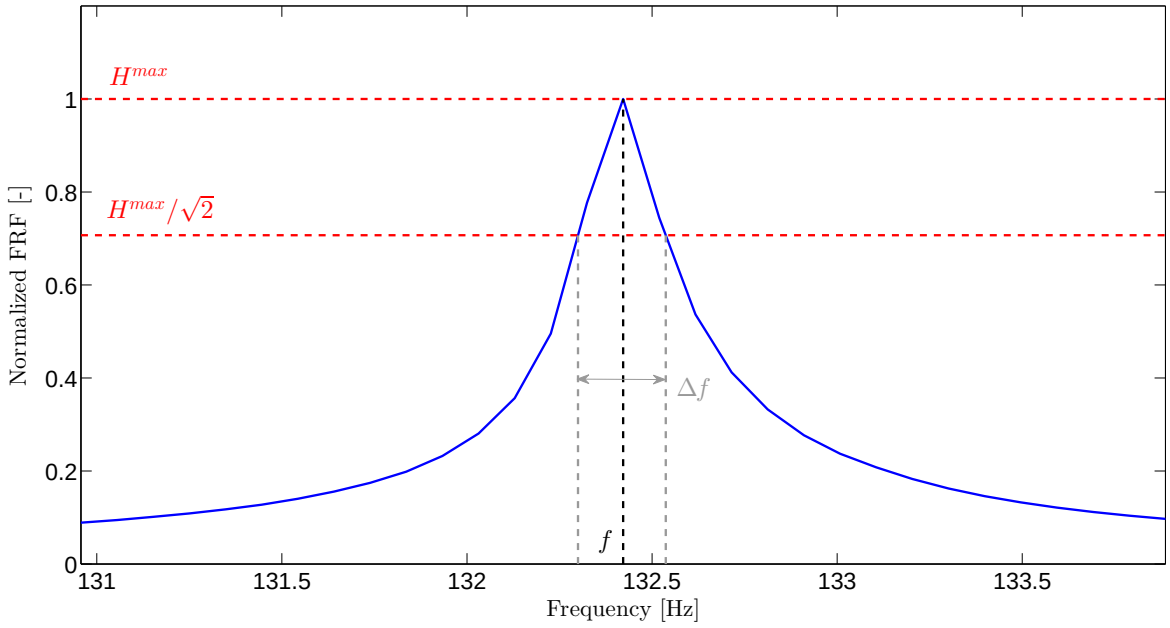

FIGURE 9 - Peak-picking method. Close-up on the fifth bending mode.

The circle-fit method is illustrated in Fig. 10 and is based on the circular nature of the Nyquist plot of the FRF when viscous damping is assumed and when the FRF is expressed in its mobility form [5]. The modal damping associated to mode k can be expressed by

$$\zeta_k = \frac{f_a^2 - f_b^2}{2f_k(f_a \tan(\theta_a/2) + f_b \tan(\theta_b/2))}, \tag{2}$$

where f_k is the natural frequency of the mode, f_a/f_b are frequencies close to f_k around the circle and θ_a/θ_b are the corresponding angles measured with respect to the radius of the cercle associated to the resonance

frequency. An example of these parameters is shown in Fig. 10. Taking different values for f_a and f_b allows to evaluate the scatter between the different estimates of the modal damping (see Fig. 11). The mean value of the different ζ computed is equal to 0.096% and is therefore in good agreement with the results of the peak-picking method.

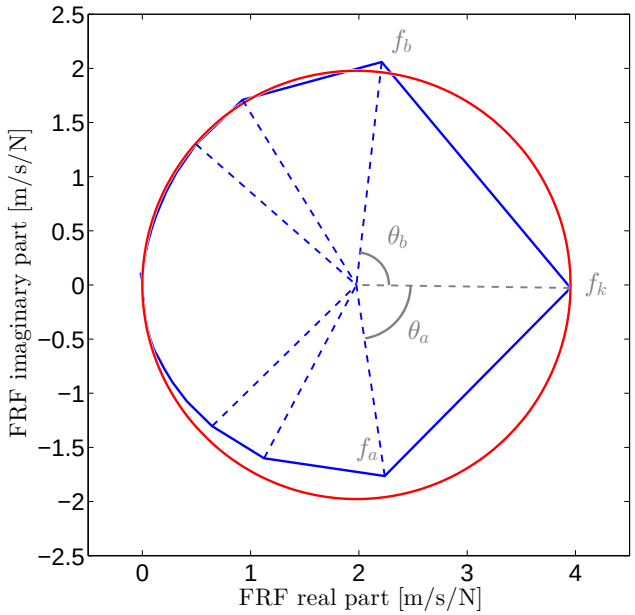

FIGURE 10 - Circle-fit method (fifth bending mode).

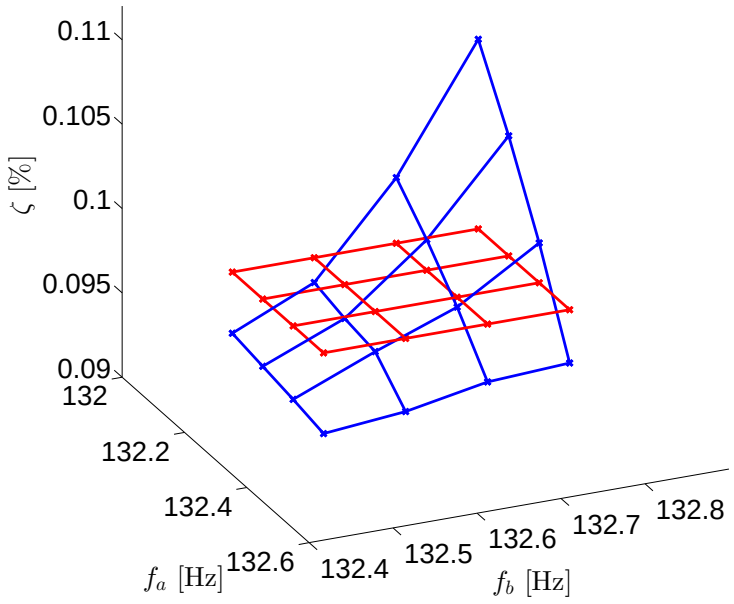

FIGURE 11 - Estimates of the fifth bending mode damping ratio obtained with the circle-fit method as a function of the frequencies f_a and f_b (Eq. 2). The red plane corresponds to the mean value.

In order to check the linearity of the structure, a second test is performed by switching the excitation and the measurement points. The structure is therefore excited at point P2 and the response is measured at point P9. Notice that the point P2 is sufficiently close to the top fixation of the strip to avoid overloading of the channels (Fig. 6). The norms of the two FRF are plotted in Fig. 12. The curves are in good agreement except at low frequencies where data suffer from noise, as already shown by the coherence function in Fig. 8. Fig. 12 shows that the reciprocity principle is verified and that the assumption of linearity is therefore justified.

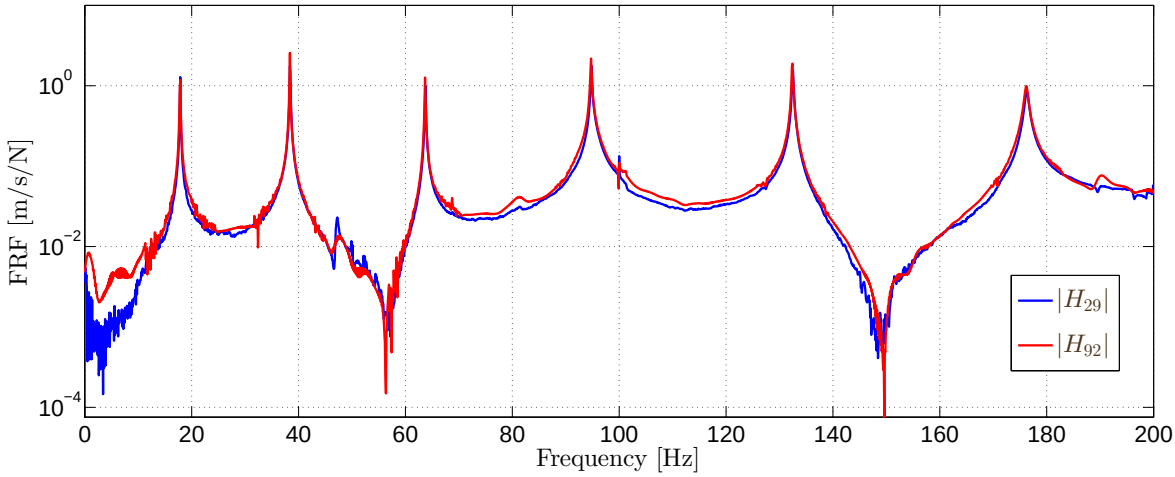

FIGURE 12 - Illustration of the reciprocity principle.

2.3 Identification process

A more detailed data acquisition is performed on the strip. The structure is excited at point P9 (see Fig. 6) and the response is successively measured at each of the other points. The values given to the various parameters used for the acquisition have already been given and justified in section 2.1. Using the measurement data, it is then possible to extract the modal parameters of the structure. On the one hand, the natural frequencies f_r and damping ratio's ζ_r are obtained using the *Least Square Complex Exponential* (LSCE) method. On the other hand, the mode shapes $\mathbf{z}_r$ are computed with the *Least Square Frequency Domain* (LSFD) method.

The LSCE method, introduced in 1979 by Brown et al. [2], works in the time domain and requires experimental measurements in the form of impulse response functions (IRF). The impulse responses functions are not directly given by the LMS Test.Lab software but are easily obtained by taking the inverse Fourier transform of the transfer functions.

An important issue of many identification techniques is the selection of the model order. The stabilization diagram allows to distinguish real modes from spurious modes. In Fig. 13, a mode is considered as "stabilized in frequency" (green marker) if its frequency differs by less than 0.1 Hz from a mode identified with the previous order. A mode is considered as "stabilized in frequency and damping" (blue marker) if it is stabilized in frequency and if its damping ratio differs by less than 0.01 % from the mode identified at this frequency at the previous order. If the mode is not stabilized in frequency, it is classified as "unstabilized" and represented by a red marker. The six modes corresponding to the peaks of the mean frequency response function (represented in gray in the figure) are clearly identified, even if the fourth and the sixth are more difficult to stabilize. Another mode is identified at 100.2 Hz. This corresponds to the torsion mode of the structure. Because the excitation and measurement points are not perfectly on the central fibre of the strip, the torsion of the strip is also excited during the tests.

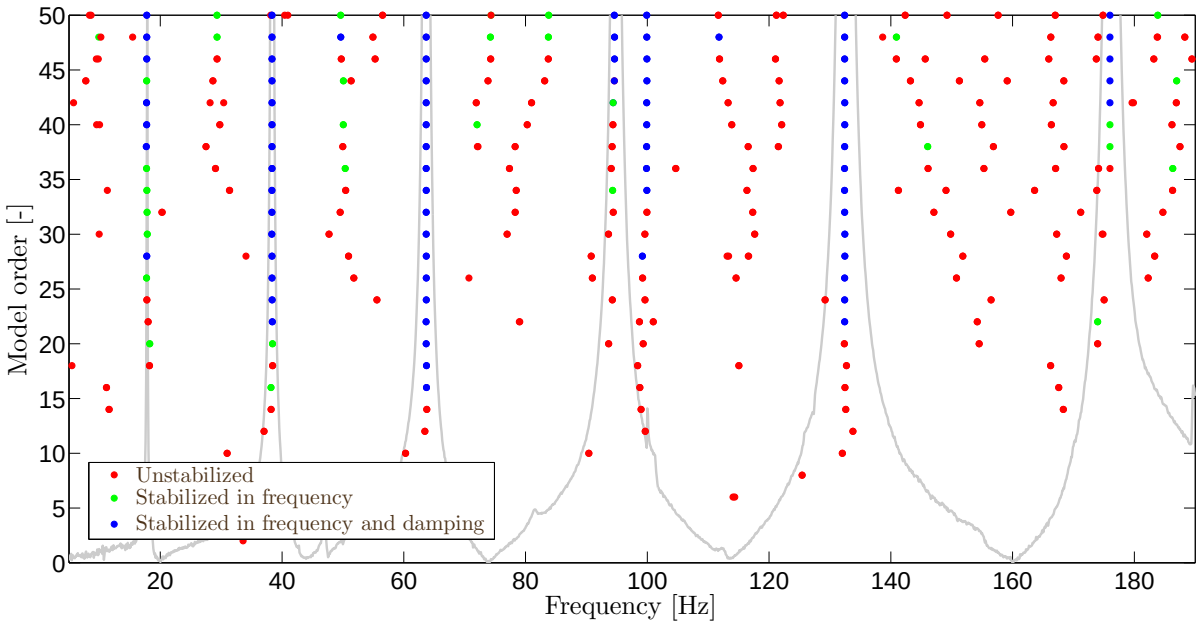

FIGURE 13 - Stabilization diagram of the LSCE method. The gray curve represents the mean frequency response function.

The eigenfrequencies and damping ratio's obtained by identification with the LSCE method are given in Table 7. It should be noted that identification methods are also directly implemented in the LMS Test.Lab software. The natural frequencies and damping ratio's obtained with the *Polyreference Least-Squares Complex Frequency-Domain* (PolyMAX) method are also listed in Table 7. A good agreement is observed between the two sets of results and gives confident in the MATLAB implementation of the LSCE method. This table shows that the damping in the structure is really light. The fourth and sixth bending modes have a modal damping larger than the other modes. These results can be compared with the results of the preliminary data acquisition described in section 2.2. On the one hand, the natural frequencies identified with the single frequency response measured (Fig. 8) are close to the frequencies of the table. On the other hand, it can also be checked that the value $\zeta = 0.09 - 0.10$ % obtained for the fifth bending mode with the peak-picking method and the circle-fit method is a good estimate of the damping ratio.

	Frequency [Hz] LSCE	*Frequency [Hz]* PolyMAX	*Damping ratio [%]* LSCE	*Damping ratio [%]* PolyMAX
Bending mode 1	17.8	17.8	0.06	0.06
Bending mode 2	38.5	38.4	0.03	0.05
Bending mode 3	63.8	63.7	0.08	0.06
Bending mode 4	94.7	94.8	0.20	0.20
Bending mode 5	132.5	132.5	0.08	0.10
Bending mode 6	175.9	176.2	0.21	0.25

TABLE 7 - Comparison of the eigenfrequencies and damping ratio's obtained with the LSCE method implemented in MATLAB and the PolyMAX method implemented in the LMS Test.Lab software.

The companion method LSFD is implemented to identify the mode shapes of the structure. Unlike the LSCE method, the LSFD method works in the frequency domain [5]. This method takes advantage of the previous knowledge of the natural frequencies and damping ratio's identified with the LSCE method (see Table 7).

The modes extracted with this method are complex. However, because the identified damping ratio's are small, one can expect that the different degrees of freedom of the structure vibrate in phase. The complexity of the mode shapes is assessed with the Argand diagram. Fig. 14 represents the Argand diagrams of the six bending modes identified with the LSFD method. It is checked in this figure that all the nodes of the structure vibrate in phase in the different mode shapes. The real bending modes extracted from the complex ones are represented in Fig. 15.

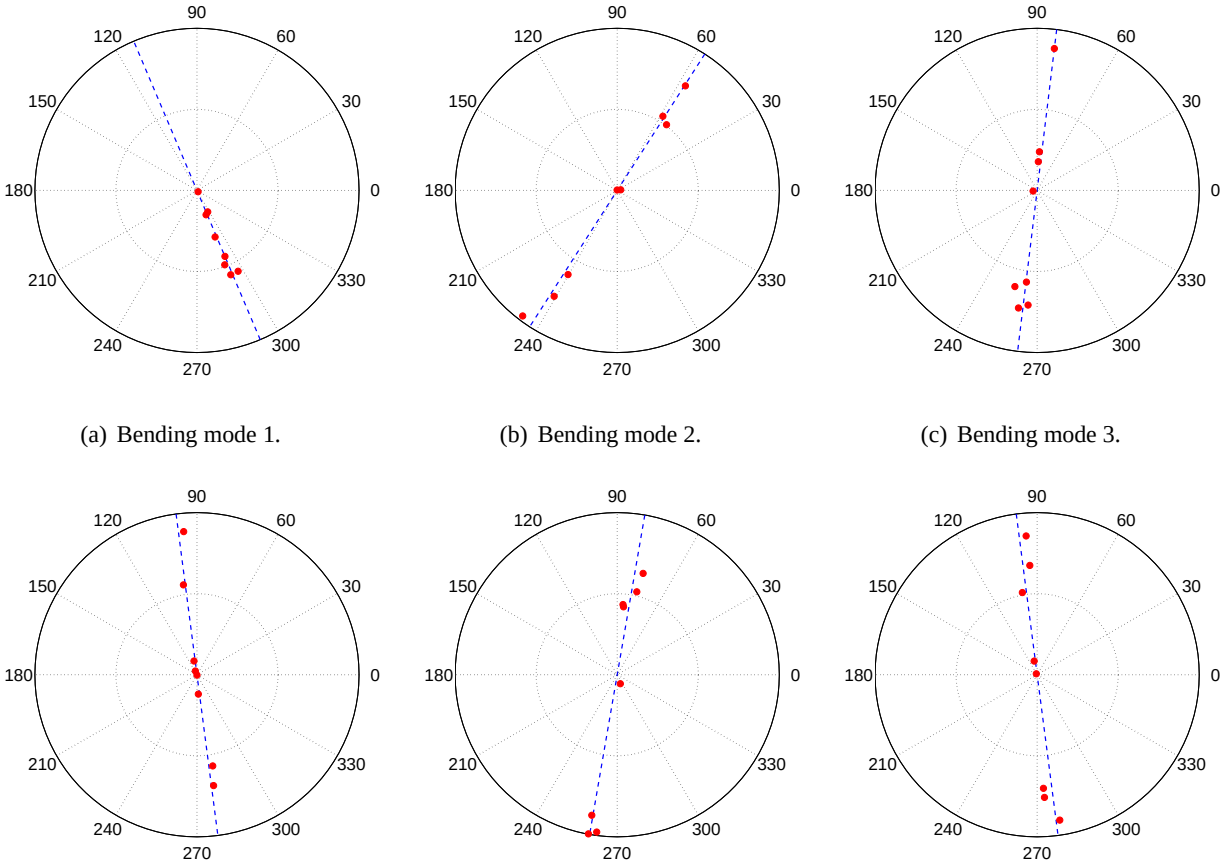

(a) Bending mode 1. (b) Bending mode 2. (c) Bending mode 3.

(d) Bending mode 4. (e) Bending mode 5. (f) Bending mode 6.

FIGURE 14 - Argand diagrams of the six first bending modes.

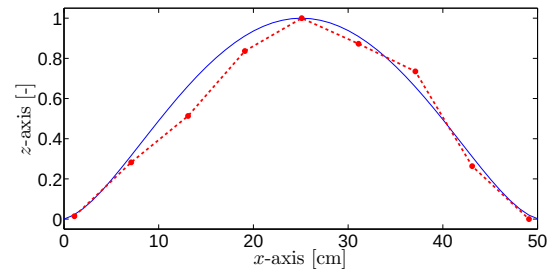

(a) First bending mode.

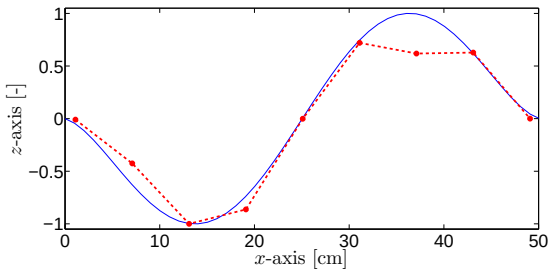

(b) Second bending mode.

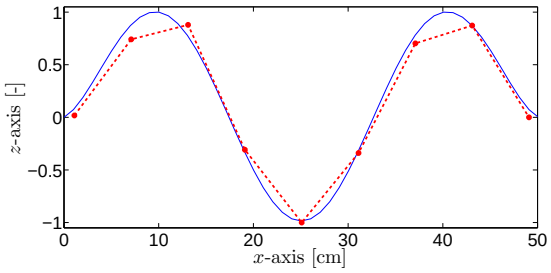

(c) Third bending mode.

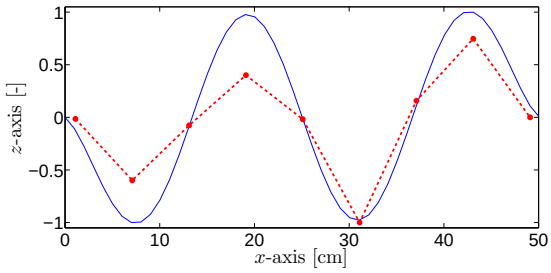

(d) Fourth bending mode.

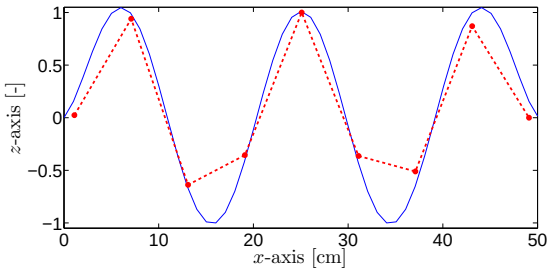

(e) Fifth bending mode.

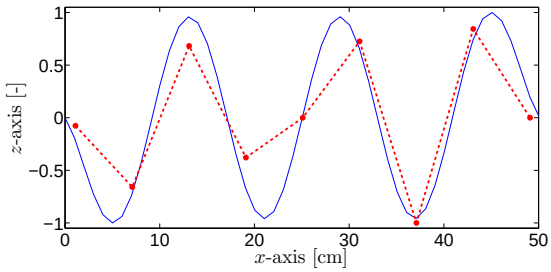

(f) Sixth bending mode.

FIGURE 15 - The six first bending modes of vibration identified with the LSFD method (in red) compared to the modes obtained with the finite element method (in blue).

Three tools are commonly used in industry in order to check that the modes are physical and, therefore, that the order is correctly selected [6].

i. The first check is provided by a visual inspection of the modes. At low frequencies, the simplest modes must be observed. This is the case here: the first modes identified correspond to the usual first bending modes of a beam.

ii. Then, the frequency response function rebuilt from the identified modal parameters has to match the measured frequency response function. Fig. 16 represents the frequency response function related to an excitation at point P9 and a response at point P3. The figure allows to compare the measured FRF with the FRF synthesized from the identified poles and modes. A good agreement is observed between the two FRF, which gives confidence in the identification process.

iii. Eventually, the different mode shapes must be independent. This is checked with the auto-MAC matrix represented in Fig. 17. Because all the out-of-diagonal terms are close to 0, the modes are indeed independent.

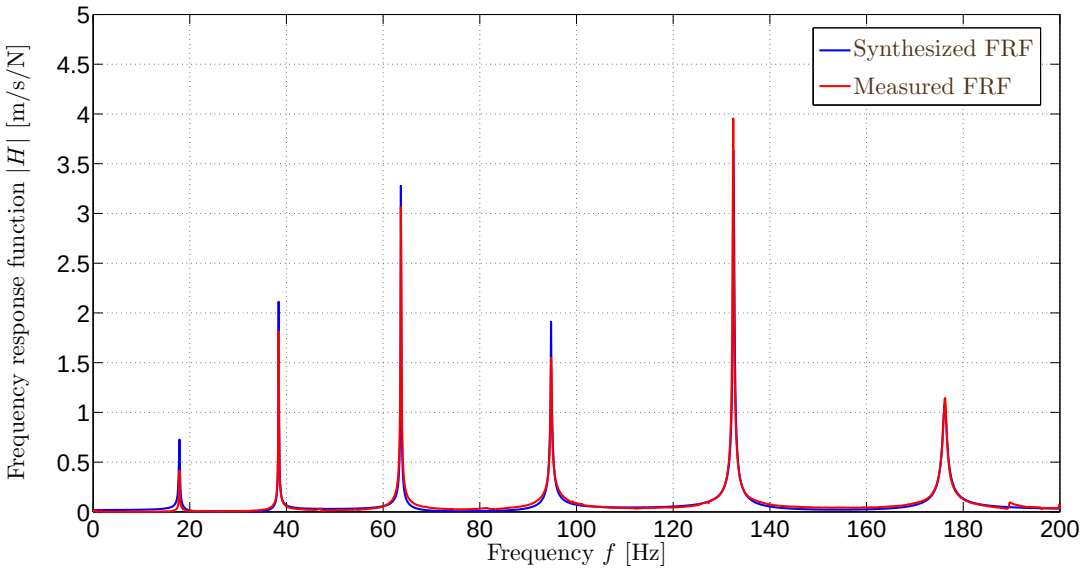

FIGURE 16 - Comparison of the synthesized and measured frequency response functions.

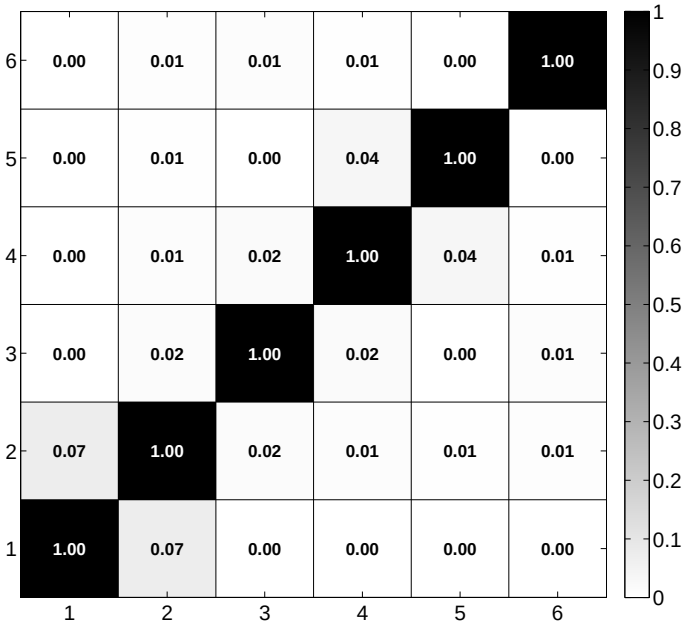

FIGURE 17 - Auto-MAC matrix of the experimental bending modes.

3 Comparison between numerical and experimental results

At this stage of the study, two sets of modal parameters are available. On the one hand, estimates of the natural frequencies and mode shapes of the strip have been obtained in section 1 based on finite element models. On the other hand, a second set of modal parameters (natural frequencies, modal damping and mode shapes) comes from the experimental modal analysis performed in section 2. In the first part of this section, the two sets of modal parameters are compared. Then, the finite element is updated in order to reduce the discrepancies between the results of the theoretical and experimental modal analyses, in agreement with the methodology set in Fig. 1.

3.1 Correlation

The results obtained with the MATLAB finite element model and with the experimental modal analysis are summarized in Table 8. The natural frequencies obtained with the initial finite element models systematically overestimate the corresponding natural frequencies identified with the experimental analysis by 3-5 %, which is clearly not acceptable.

	Frequency [Hz] TMA	*Frequency [Hz]* EMA	*Relative error [%]*
Bending mode 1	18.4	17.8	3.4
Bending mode 2	39.8	38.5	3.4
Bending mode 3	66.1	63.8	3.6
Bending mode 4	98.7	94.7	4.2
Bending mode 5	137.9	132.5	4.1
Bending mode 6	184.2	175.9	4.7

TABLE 8 - Comparison of the eigenfrequencies obtained from theoretical (TMA, initial model) and experimental (EMA) modal analyses.

Visually, the two sets of mode shapes are in good agreement (see Fig. 3 and 15). They correspond to the successive bending modes of the strip. The Modal Assurance Criterion (MAC) can be used to quantify the correlation between the two sets of modes [3]. The MAC computed between mode i of the first family $\psi^1_{(i)}$ and mode j of the second $\psi^2_{(j)}$ is given by

$$\mathrm{MAC}(\psi^1_{(i)}, \psi^2_{(j)}) = \left(\frac{{\psi^1_{(i)}}^T \psi^2_{(j)}}{||\psi^2_{(j)}|| \cdot ||\psi^2_{(j)}||} \right)^2 . \tag{3}$$

The MAC matrix based on the two sets of modes available is represented in Fig. 18. The close-to-one values of its diagonal elements and the negligible values of its out-of-diagonal elements confirm the correlation observed previously.

In conclusion, despite the high correlation between the mode shapes, a model updating is required to decrease the relative errors between the natural frequencies.

3.2 Model updating

The poor agreement can result from a bad experimental analysis or from modeling errors and uncertainties. It has been shown in the previous section that the measurement process is performed in a rigorous way and

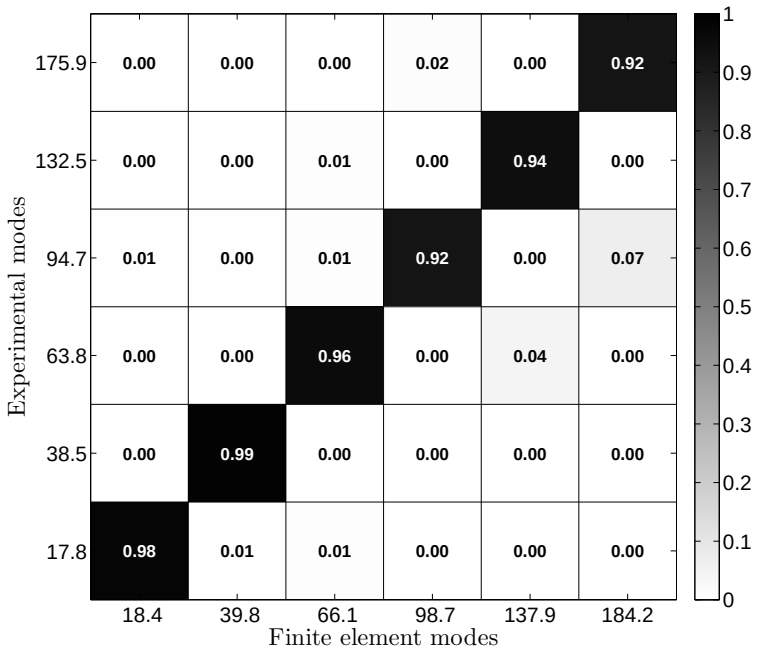

FIGURE 18 - MAC matrix between the numerical modes (initial model) and the experimental modes.

that the choice of the measurement coordinates is justified. Moreover, the modal identification gives the same results as the PolyMAX identification method implemented directly in the LMS Test.Lab software. It is therefore argued that it is the finite element modeling of the structure that must be improved.

The inaccuracies in the finite element modeling come from three main sources. In the following, the modeling uncertainties about physical and geometrical parameters and the discretization and approximation errors are successively considered.

In order to identify possible errors on the geometry of the structure, new measurements of the dimensions of the structure are done. Two 30 cm samples of the steel strip are weighted to correct the steel density. The pre-stress mass is also precisely weighted. Eventually, a tensile test is performed on the two samples of the strip to revise the estimate of the Young's modulus. The corresponding updated values of the geometrical and material properties are listed in Tables 9 and 10.

Parameter	*Symbol*	*Value*	*Units*
Length	l	50.1	cm
Width	w	25	mm
Thickness	t	0.4	mm
Pre-stress mass	m	1.816	kg

TABLE 9 - Geometrical properties of the steel structure (corrected).

While errors can be introduced by the process of discretization, it was shown in the first section that the

Parameter	*Symbol*	*Value*	*Units*
Density	ρ	7,767	kg/m^3
Young's modulus	E	2.06	GPa
Poisson's ratio	ν	0.33	[-]

TABLE 10 - Material properties of the steel structure (corrected).

number of finite elements used in the numerical models is sufficient to capture the dynamics of the problem. Refining the mesh does not lead to any significant change in the natural frequencies.

The approximation errors are related to assumptions about the physics of the model. Here, the natural frequencies obtained with the model are slightly higher than the experimental ones. The model is therefore too rigid with respect to reality. This can be ascribed to the choice of the boundary conditions in the initial model described in section 1. Perfect clamping is a mathematical idealization that never exists in practice. It is impossible to completely prevent any rotation about the *y*-axis at the fixations of the strip (see Fig. 2). The finite element model is therefore corrected by introducing a stiffness in rotation about the *y*-axis at both ends of the strip. To simplify the analysis, the stiffness coefficient is supposed to be the same on both sides. The rigidity of the clamping is determined in such a way that it minimizes the error (in a least-square sense) between the natural frequencies coming from the numerical and the experimental modal analyses. Fig. 19 represents the global error as a function of the stiffness in rotation k. A optimum value of $k = 3.83$ Nm/rad is found.

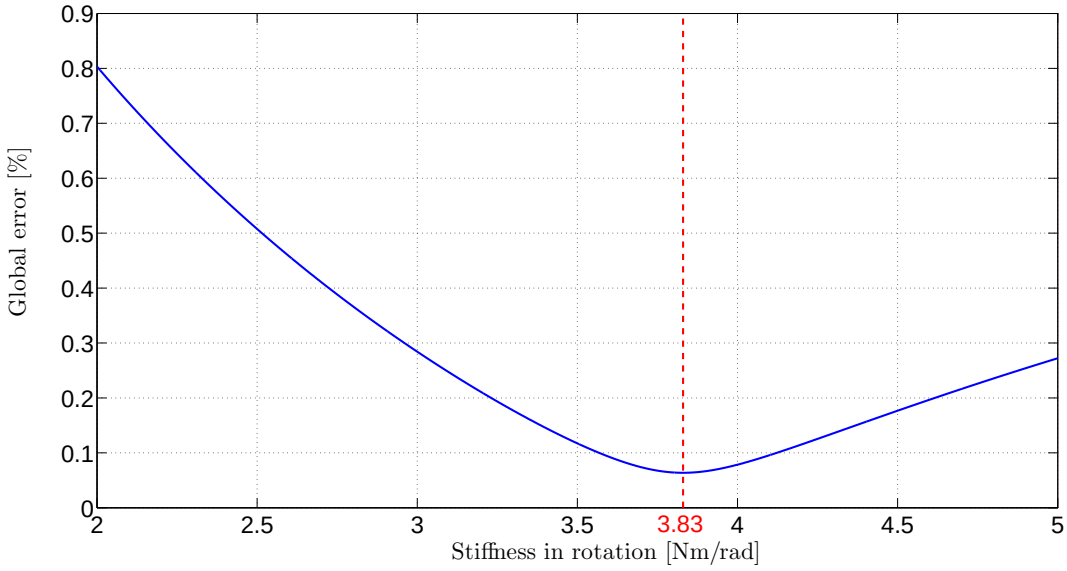

FIGURE 19 - Global error on the natural frequencies as a function of the stiffness in rotation.

Table 11 shows the natural frequencies computed after updating of the finite element model, *i.e.* after correction of the material/geometrical properties of the strip and modification of the boundary conditions. These frequencies can be compared with the experimental frequencies and show now relative errors less than 0.2%.

	Frequency [Hz] TMA	*Frequency [Hz]* EMA	*Relative error [%]*
Bending mode 1	17.8	17.8	0.1
Bending mode 2	38.5	38.5	0.1
Bending mode 3	63.7	63.8	0.1
Bending mode 4	94.8	94.7	0.1
Bending mode 5	132.2	132.5	0.2
Bending mode 6	176.3	175.9	0.2

TABLE 11 - Comparison of the eigenfrequencies obtained from theoretical (TMA, after updating of the model) and experimental (EMA) modal analyses.

One can also check in Fig. 20 that the adjustment of the model does not have any detrimental effect on the correlation between the numerical and experimental mode shapes. The out-of-diagonal terms are really close to 0 while the diagonal terms vary between 0.96 and 0.99.

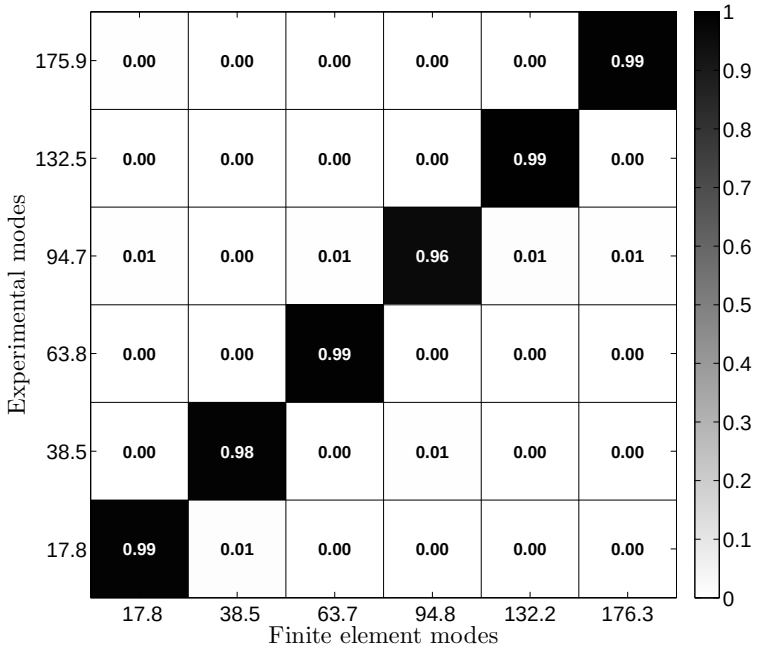

FIGURE 20 - MAC matrix between the numerical modes (corrected model) and the experimental modes.

Conclusion

Throughout this project, several theoretical and experimental aspects of modal analysis have been addressed in order to study a pre-stressed steel strip. The modal analysis theory relies on two main assumptions: linearity and time invariance of the structure.

As a first step, finite element models of the strip have been built in MATLAB and SAMCEF Field. They have been used to carry out the theoretical modal analysis of the structure and to identify a first set of modal parameters (natural frequencies and mode shapes) related to the six first bending mode of the strip and the first torsion mode. Because models are always synonymous with approximations and uncertainties, they must be validated against experimental data. Testing of the real structure and identification methods have allowed to extract the real modal parameters of the strip. First, a single measured frequency response function has provided a quick way of determining the number of modes in the studied frequency bandwidth. Two one-degree of freedom methods, namely the *Peak-Picking* method and the *Circle-Fit* method, have provided first estimates of the damping ratio's. Then, the *Least Square Complex Exponential* and *Least Square Frequency Domain* methods have been used to identify in an accurate way the modal parameters of the structure. Experimental modal analysis has also allowed to get a much better knowledge of the modal damping. Eventually, the finite element model has been updated in order to represent in a much more accurate way the real structure and, in particular, its modal characteristics.

This reliable finite element model can now be used to study the dynamics of the real structure in a much faster and more flexible way than through experimental measurements. Contrary to experimental measurements, which only provide information about a limited number of points on the structure, the finite element model can describe the whole structure. Moreover, it allows to assess the impact of changes in geometrical and material properties without the need to build a new prototype.

References

[1] ASHBY M., *Materials Selection in Mechanical Design*, Elsevier, Oxford (2005).

[2] BROWN D.L., ALLEMANG R.J., ZIMMERMAN R., MERGEAY M., *Parameter estimation techniques for modal analysis.* SAE Technical Paper Series No. 790221 (1979).

[3] EWINS D. J., *Modal Testing: Theory, Practice and Application*, 2nd edition, Research Studies Press Ltd (2000).

[4] GERADIN M., RIXEN D. J., *Mechanical Vibrations : Theory and Application to Structural Dynamics*, third edition, Wiley (2015).

[5] MAIA N., SILVA J., HE J., LIEVEN J., LIN R.-M., SKINGLE G., TO W., URGUEIRA A., *Theoretical and Experimental Modal Analysis*, Research Studies Press Ltd (1997).

[6] LMS Test.Lab official website: `https://www.plm.automation.siemens.com/fr/products/lms/testing/test-lab/index.shtml` (Last view November 5th, 2017).